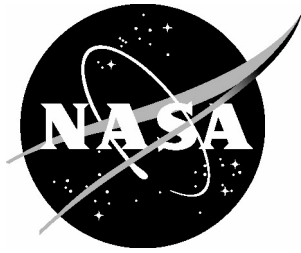


NASA/CR-2005-213780



Empirical Prediction of Aircraft Landing Gear Noise

Yueping Guo
Boeing Phantom Works, Long Beach, California

July 2005

The NASA STI Program Office . . . in Profile

Since its founding, NASA has been dedicated to the advancement of aeronautics and space science. The NASA Scientific and Technical Information (STI) Program Office plays a key part in helping NASA maintain this important role.

The NASA STI Program Office is operated by Langley Research Center, the lead center for NASA's scientific and technical information. The NASA STI Program Office provides access to the NASA STI Database, the largest collection of aeronautical and space science STI in the world. The Program Office is also NASA's institutional mechanism for disseminating the results of its research and development activities. These results are published by NASA in the NASA STI Report Series, which includes the following report types:

- **TECHNICAL PUBLICATION.** Reports of completed research or a major significant phase of research that present the results of NASA programs and include extensive data or theoretical analysis. Includes compilations of significant scientific and technical data and information deemed to be of continuing reference value. NASA counterpart of peer-reviewed formal professional papers, but having less stringent limitations on manuscript length and extent of graphic presentations.
- **TECHNICAL MEMORANDUM.** Scientific and technical findings that are preliminary or of specialized interest, e.g., quick release reports, working papers, and bibliographies that contain minimal annotation. Does not contain extensive analysis.
- **CONTRACTOR REPORT.** Scientific and technical findings by NASA-sponsored contractors and grantees.

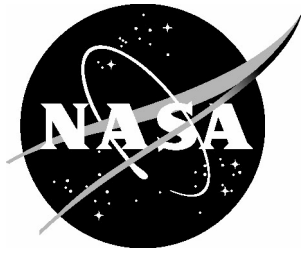
- **CONFERENCE PUBLICATION.** Collected papers from scientific and technical conferences, symposia, seminars, or other meetings sponsored or co-sponsored by NASA.
- **SPECIAL PUBLICATION.** Scientific, technical, or historical information from NASA programs, projects, and missions, often concerned with subjects having substantial public interest.
- **TECHNICAL TRANSLATION.** English-language translations of foreign scientific and technical material pertinent to NASA's mission.

Specialized services that complement the STI Program Office's diverse offerings include creating custom thesauri, building customized databases, organizing and publishing research results ... even providing videos.

For more information about the NASA STI Program Office, see the following:

- Access the NASA STI Program Home Page at <http://www.sti.nasa.gov>
- E-mail your question via the Internet to help@sti.nasa.gov
- Fax your question to the NASA STI Help Desk at (301) 621-0134
- Phone the NASA STI Help Desk at (301) 621-0390
- Write to:
NASA STI Help Desk
NASA Center for AeroSpace Information
7121 Standard Drive
Hanover, MD 21076-1320

NASA/CR-2005-213780



Empirical Prediction of Aircraft Landing Gear Noise

Yueping Guo
Boeing Phantom Works, Long Beach, California

National Aeronautics and
Space Administration

Langley Research Center
Hampton, Virginia 23681-2199

Prepared for Langley Research Center
under Contract NAS1-00086

July 2005

Available from:

NASA Center for AeroSpace Information (CASI)
7121 Standard Drive
Hanover, MD 21076-1320
(301) 621-0390

National Technical Information Service (NTIS)
5285 Port Royal Road
Springfield, VA 22161-2171
(703) 605-6000

Table of Contents

1. Nomenclature, List of Tables, List of Figures	2
2. Introduction.....	5
3. Theoretical Basis.....	7
4. Scaling Laws	11
5. Empirical Prediction Schemes	13
6. Normalized Spectra.....	17
7. Directivity Factors	20
8. Complexity Factor	22
9. Validation.....	25
10. Conclusions and Discussions.....	31
11. Acknowledgments.....	32
12. References.....	32

1. Nomenclature, List of Tables, List of Figures

A	= amplitude of normalized spectra
B	= parameter defining normalized spectra
D	= directivity factor
$EPNL$	= Effective Perceived Noise Level
F	= normalized spectrum
L	= total length of struts
L_j	= length of j th strut
M	= Mach number of mean flow ahead of landing gear
M_0	= Flight Mach number
N_s	= number of struts
N_w	= number of wheels
$OASPL$	= overall sound pressure level
R	= radial distance of far field microphone
S	= aggregate surface integration effects
SPL	= sound pressure level
St	= Strouhal number
U	= mean flow velocity
W	= aircraft takeoff gross weight
a	= average cross section dimension of struts
a_j	= linear dimension of j th strut cross section
b_j	= linear dimension of j th strut cross section
c_0	= constant sound speed
d	= wheel diameter
d_s	= diameter of shock strut
f	= frequency
h	= parameter defining directivity factor
k_0	= acoustic wavenumber
n_i	= i th component of surface normal
p	= sound pressure
p_s	= surface pressure
s_j	= perimeter of the j th strut cross section
t	= time
u_0	= velocity scale
w	= width of landing gear wheels
\mathbf{x}	= far field coordinate vector
\mathbf{y}	= near field coordinate vector
Δ	= Doppler factor
Π	= far field noise power spectral density

Π_s	= surface pressure power spectral density
α	= coefficient of atmospheric absorption
β	= radiation efficiency
γ	= wheel track alignment angle
l	= typical size of small details
l_0	= length scale
η	= complexity factor
μ	= controlling high frequency falloff
θ	= emission angle in flyover plane
ρ_0	= constant mean density
σ	= power index in normalized spectra
τ	= source time
τ_0	= time scale
ω	= angular frequency
ω_d	= Doppler shifted angular frequency

Table 1 Functional dependencies of landing gear component noise.

Table 2 Empirical amplitudes of the three landing gear noise components.

Table 3 Parameters to define the normalized spectra for the three landing gear noise components.

Table 4 Parameters defining the directivities of the three landing gear noise components.

Table 5 Examples of maximum gross takeoff weight for some aircraft types.

Table 7 Typical dimensions of the main struts in the Boeing 737 main landing gear.

Table 6 Examples of wheel parameters.

Table 8 Typical dimensions of the main struts in the Boeing 777 main landing gear.

Table 9 Typical dimensions of main struts in the Boeing 777 nose gear assembly.

Figure 1 Illustration of the landing gear geometry and definitions of the coordinate system.

Figure 2 Illustration of the normalized power spectral density in the low, mid and high frequency domain.

Figure 3 One third octave band levels of the three power spectral densities shown in Figure 2 respectively for the three frequency domains.

Figure 4 Models of the directivity factors for the three spectral components of landing gear noise.

Figure 5 Comparison of empirical model with test data for the directivity of high frequency landing gear noise.

Figure 6 Overall far field directivity of the Boeing 777 landing gear noise.

Figure 8 Increment of landing gear high frequency noise due to gear complexity.

Figure 7 Increment of landing gear high frequency noise due to wheel track alignment angle.

Figure 9 Comparison of SPL between predictions and test data for an isolated Boeing 737 main landing gear.

Figure 10 An example of spectral decomposition of total noise for the Boeing 737 main landing gear.

Figure 11 Comparison of OASPL between predictions and test data for an isolated Boeing 737 main landing gear.

Figure 12 Comparison of landing gear noise SPL between predictions and test data for the Boeing 777 aircraft.

Figure 13 An example of the Boeing 777 aircraft landing gear noise and the contributions from its main and nose gear.

Figure 14 Comparison of OASPL between prediction and flight test data for the Boeing 777 landing gear noise.

2. Introduction

Because of the geometric and flow complexity, landing gear noise prediction has mostly been empirical (Ref 1 to 8). In most cases, a particular database for a landing gear configuration is used to derive parametric trends and prediction schemes. The empirical approach has certainly proven to be valuable in practical applications. Its limitations and drawbacks, however, are also well recognized, of which, the limited parametric range in a particular database and the error in the measurements are probably two of the most severe obstacles in empirical modeling. The former limits the validity domain of the empirical prediction, because of the uncertainties outside the database used to develop the prediction methods, while the latter can lead to wrong or inaccurate parametric trends, if the empirical tools are developed by blunt-force data collapsing. Thus, it is important in empirical tool development to constantly update the tools, both by introducing physics-based theory into the modeling so that general scaling laws are utilized to cover a wide range of flow and geometry parameters, and by incorporating new database into the prediction schemes. This is what has motivated the work reported here, and our objective is to take a step forward from existing empirical methods to develop improved schemes for landing gear noise prediction.

We will start with the scaling laws from the theory of aerodynamic noise generation, which identify general trends such as the sixth power law of the Mach number dependence and the inverse fourth power convective amplification (Ref 9 to 13). This gives the empirical schemes a sound theoretical foundation. The methods are, however, heavily empirical because the scaling laws will be correlated to available databases so that parameters in the scaling laws will be quantitatively determined and the predictions are not only for the general parametric trends, but also for the absolute noise levels. To overcome the limitations and drawbacks of any particular set of data, we will make use of all the published data, which includes the early studies as well as recent data (Ref 6, 7 and Ref 15 to 21). Furthermore, the empirical models will also be calibrated with recent results from numerical simulations (Ref 22 to 26), which, though not directly applicable for practical predictions, provide valuable understanding and insight of the noise characteristics of landing gears, especially in the low and mid frequency domain.

This semi-analytical and semi-empirical approach will be applied to three spectral components of the landing gear noise, namely, the low, the mid and the high frequency noise. The decomposition of landing gear noise into three spectral components has been discussed before (Ref 6, 7 and 13). It results from detailed analyses of landing gear noise test data, which have revealed different characteristics of the measured noise in each individual frequency domains, such as their spectral features, their far field directivities and their dependencies on the geometric parameters of the gear assembly. The decomposition also reflects the source mechanisms of the noise in different frequency domains; the three groups of landing gear parts, namely, the wheels, the main struts and the small details, have typical sizes that significantly differ from each other. These distinctively different length scales lead to sound generation in

distinctively different frequency domains, supporting the hypothesis that the total landing gear noise is the incoherent summation of the three spectral components.

For all three spectral components, we will derive normalized spectra to define the frequency features of the noise, in term of the Strouhal number based on the flow velocity upstream of the landing gear, which is known to be different from the free stream velocity or the aircraft flight velocity, and the respective length scales of the three groups of landing gear parts. General features of the normalized spectra include the unity maximum at some values of the Strouhal number and the falloff spectral shapes at both low and high frequencies. The spectra have different widths, from the narrowest for the low frequency component to the widest for the high frequency component, reflecting the different size distributions of the three groups of landing gear parts. The wheels have the same size so that the low frequency noise from the wheels is narrowly confined to frequencies near the vortex shedding frequency of the wheels. For noise from the main struts that have various sizes, the spectrum has a broad hump. The spectral hump becomes even broader for the high frequency noise because many different sizes are included in the group of small features that generate high frequency noise. Directivity factors will also be derived for all three noise components, which have unity minimum at 90 degrees of emission angle and higher values at other angles with maximum in the upstream and downstream direction. The angular variations are greatest for the high frequency components and almost flat for the low frequency noise.

The amplitude of each of the three noise components will be determined by geometric and flow quantities unique to the corresponding group of landing gear parts, together with functional dependencies that are common to all three components. The common features are the Mach number dependence, the spherical spreading, the convective amplification and the atmospheric absorption. For landing gear noise that is usually at low Mach numbers, the dominant noise sources are the pressure fluctuations on the surfaces of the landing gear parts, according to the theory of aerodynamic sound (Ref 9 to 13). Thus, one component-dependent feature is the aggregate effect of surface pressures integrated over the surfaces of the landing gear parts. For the low and mid frequency component, this effect will be deterministically defined by the dimensions of the wheels and main struts, respectively. For the high frequency noise associated with small geometric features in the gear assembly, the large number of irregularly shaped parts makes it impractical to count and define the sizes and shapes of all the small parts. Thus, we will introduce a complexity factor to account for the small parts, which can be regarded as a statistical description of the sources of high frequency landing gear noise. We will discuss geometric and flow parameters that affect this complexity factor and an empirical definition will be given for noise prediction of practical landing gears.

To validate the prediction schemes and demonstrate their practical applications, the empirical models developed here will be applied to the landing gear noise of the Boeing 737 and 777 aircraft. For the Boeing 737 aircraft, the predictions will be compared with wind tunnel test data for an isolated main landing gear, at various flow conditions and emission angles. For the

Boeing 777 aircraft, comparisons will be done with flight test data at various emission angles, which include contributions from both the main gears and the nose gear. In both cases, comparisons between predictions and data show good agreements; the empirical models not only capture the parametric trends of the noise measurements, but also accurately predict the absolute noise levels.

3. Theoretical Basis

Our empirical prediction schemes for landing gear noise are based on the scaling laws of the theory of aerodynamic noise generation. The general theory of sound generation by moving bodies have been extensively studied in the past (Ref 9 to 13), but for completeness and for the convenience of discussions, they are briefly derived here, with particular reference to landing gear noise. We consider a landing gear assembly moving at constant speed U in the positive x_1 -direction, where the coordinate system $\mathbf{x} = \{x_1, x_2, x_3\}$ is fixed in relation to the far field microphones. The geometry and coordinate system are illustrated in Figure 1.

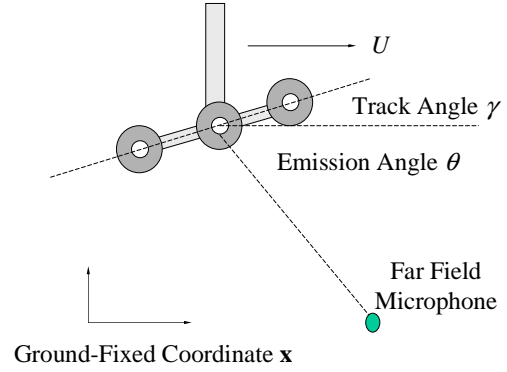


Figure 1 Illustration of the landing gear geometry and definitions of the coordinate system.

The source locations on the landing gear are denoted by $\mathbf{y} = \{y_1, y_2, y_3\}$, which is related to the coordinate system fixed on the landing gear assembly by

$$\mathbf{y} = \boldsymbol{\eta} + \int_0^{\tau} \mathbf{U} d\tau = \boldsymbol{\eta} + \mathbf{U}\tau, \quad (3.1)$$

where $\boldsymbol{\eta} = \{\eta_1, \eta_2, \eta_3\}$ is the body-fixed coordinate system, τ is the time measuring the source process and $\mathbf{U} = U \hat{x}_1$ is the constant velocity in the x_1 -direction, the overhead hat on x_1 denoting unit vector.

The far field sound pressure due to the landing gear assembly can be conveniently expressed by the Ffowcs Williams/Hawking equation (Ref 9). For low Mach number flows, as is the case for landing gear noise applications where the typical flow Mach number is about 0.2, the dominant sound is assumed to be given by the dipole term due to surface pressure fluctuations. In this case, the sound pressure $p(\mathbf{x}, t)$, as a function of the microphone location \mathbf{x} and receiving time t , can be written as

$$p(\mathbf{x}, t) = \frac{1}{4\pi} \frac{\partial}{\partial x_i} \int_{s(\boldsymbol{\eta})} \frac{n_i p_s(\boldsymbol{\eta}, \tau)}{|\mathbf{x} - \mathbf{y}|(1 - M\hat{x}_1)} d^2\boldsymbol{\eta}. \quad (3.2)$$

Here p_s is the surface pressure on the moving landing gear parts whose surfaces are collectively denoted by S and we have introduced $M = U/c_0$ to denote the Mach number with c_0 being the constant sound speed. The unit normal of the surface, pointing into the flow, is denoted by n_i , with the repeated indices implying tensor summation. The surface integration is to be carried out in the body-fixed coordinate system $\boldsymbol{\eta}$ in which the landing gear geometry is time-invariant. The source time τ is now given by the retarded time, defined by the implicit equation

$$\tau = t - |\mathbf{x} - \boldsymbol{\eta} - \mathbf{U}\tau| / c_0. \quad (3.3)$$

This equation can be readily solved to find the source time in terms of the coordinate variables and the receiver time,

$$\tau = t - \frac{\left(M^2 (x_1 - \eta_1 - Ut)^2 + (1 - M^2) |\mathbf{x} - \boldsymbol{\eta} - \mathbf{U}t|^2 \right)^{1/2} + M(x_1 - \eta_1 - Ut)}{c_0(1 - M^2)}. \quad (3.4)$$

For the purpose of deriving the far field sound pressure, we assume that the microphones are located far away from the landing gear so that

$$|\mathbf{x}| \gg |\mathbf{y}|. \quad (3.5)$$

In this case, the implicit equation (3.3) can be expanded in powers of $1/|\mathbf{x}|$, which leads to

$$\tau = t - \frac{|\mathbf{x}|}{c_0} + \frac{\boldsymbol{\eta} \cdot \mathbf{x}}{c_0 |\mathbf{x}|} + M \hat{x}_1 \tau. \quad (3.6)$$

Thus, the explicit solution for τ becomes

$$\tau = \frac{1}{\Delta} \left(t - \frac{|\mathbf{x}|}{c_0} + \frac{\boldsymbol{\eta} \cdot \mathbf{x}}{c_0 |\mathbf{x}|} \right), \quad (3.7)$$

where Δ stands for the Doppler factor defined by

$$\Delta = 1 - \frac{\mathbf{U} \cdot \mathbf{x}}{c_0 |\mathbf{x}|} = 1 - M \hat{x}_1 = 1 - M \cos \theta, \quad (3.8)$$

where we have introduced the emission angle θ which is measured from the upstream direction of the flight path, as illustrated in Figure 1.

The far field assumption can be used to simplify the sound pressure given by (3.2). Under the condition (3.5), the spatial derivative in (3.2) can be replaced with a time derivative

$$\frac{\partial}{\partial x_i} = -\frac{\hat{x}_i}{c_0} \frac{\partial}{\partial t}, \quad (3.9)$$

and the spherical spreading of the sound propagation can be approximated as

$$\frac{1}{|\mathbf{x} - \mathbf{y}|} = \frac{1}{|\mathbf{x}|} = \frac{1}{R}. \quad (3.10)$$

Thus, the sound pressure (3.2) simplifies to

$$p(\mathbf{x}, t) = -\frac{\hat{x}_i}{4\pi c_0 R \Delta} \frac{\partial}{\partial t} \int_{S(\boldsymbol{\eta})} n_i p_s(\boldsymbol{\eta}, \tau) d^2 \eta. \quad (3.11)$$

This result can now be converted to frequency domain by taking Fourier transform on both sides according to the definition

$$\tilde{p}(\mathbf{x}, \omega) = \int_t p(\mathbf{x}, t) e^{i\omega t} dt \quad \text{and} \quad p(\mathbf{x}, t) = \frac{1}{2\pi} \int_{\omega} \tilde{p}(\mathbf{x}, \omega) e^{-i\omega t} d\omega, \quad (3.12)$$

where ω is the angular frequency and the overhead tilde denotes quantities in the Fourier transform domain. When (3.12) is applied to (3.11), the left-hand side gives the Fourier transform of the far field sound pressure. For the right hand side, the transform of the surface pressures at the source time τ can be facilitated by making use of the result (3.7) for the retarded time and

$$\begin{aligned} \int_t p_s(\boldsymbol{\eta}, \tau) e^{i\omega t} dt &= \Delta e^{ik_0 R} e^{-ik_0 \boldsymbol{\eta} \cdot \hat{\mathbf{x}}} \int_{\tau} p_s(\boldsymbol{\eta}, \tau) e^{i\omega_d \tau} d\tau \\ &= \Delta e^{ik_0 R} e^{-ik_0 \boldsymbol{\eta} \cdot \hat{\mathbf{x}}} \tilde{p}_s(\boldsymbol{\eta}, \omega_d). \end{aligned} \quad (3.13)$$

Here, we have introduced the acoustic wave number k_0 to save writing, which is defined by $k_0 = \omega / c_0$, and ω_d is the Doppler-shifted angular frequency, which is related to ω by $\omega_d = \omega \Delta$. With this, the far field pressure (3.11) becomes

$$\tilde{p}(\mathbf{x}, \omega) = \frac{ik_0 \hat{x}_i}{4\pi R} e^{ik_0 R} \int_{S(\boldsymbol{\eta})} n_i \tilde{p}_s(\boldsymbol{\eta}, \omega_d) e^{-ik_0 \boldsymbol{\eta} \cdot \hat{\mathbf{x}}} d^2 \eta. \quad (3.14)$$

Thus, the far field sound pressure at frequency ω is related to the surface pressures at the Doppler-shifted frequency ω_d . This shift in frequency between the surface pressures and the far field sound pressure is due to the effects of the motion (with velocity \mathbf{U}) of the landing gear.

The noise spectrum (power spectrum density) can be derived from the far field pressure by multiplying it by its complex conjugate and taking the ensemble average of the result. By denoting the noise spectrum by Π , we have the definition

$$\Pi(\mathbf{x}, \omega) \delta(\omega - \omega') = \langle \tilde{p}(\mathbf{x}, \omega) \tilde{p}^*(\mathbf{x}, \omega') \rangle, \quad (3.15)$$

where the asterisk denotes complex conjugate and the bracket $\langle \dots \rangle$ implies ensemble average. From this, a trivial integration with respect to ω' leads to

$$\Pi(\mathbf{x}, \omega) = \int_{\omega'} \langle \tilde{p}(\mathbf{x}, \omega) \tilde{p}^*(\mathbf{x}, \omega') \rangle d\omega'. \quad (3.16)$$

By substituting the far field sound pressure (3.14) into this, we have

$$\Pi(\mathbf{x}, \omega) = \frac{\hat{x}_i \hat{x}_j}{(4\pi R)^2} \int_{s'} \int_{s'} n_i n'_j \int_{\omega'} k k' e^{i(k_0 - k'_0)R} \langle \tilde{p}_s(\boldsymbol{\eta}, \omega_d) \tilde{p}_s^*(\boldsymbol{\eta}', \omega'_d) \rangle e^{i(k'_0 \boldsymbol{\eta}' - k_0 \boldsymbol{\eta}) \cdot \hat{\mathbf{x}}} d\omega'_d d^2 \boldsymbol{\eta} d^2 \boldsymbol{\eta}'. \quad (3.17)$$

The integration with respect to ω' can be carried out by making use of the relation (3.15) applied to the surface pressures, namely,

$$\Pi_s(\boldsymbol{\eta}, \boldsymbol{\eta}', \omega_d) \delta(\omega_d - \omega'_d) = \langle \tilde{p}_s(\boldsymbol{\eta}, \omega_d) \tilde{p}_s^*(\boldsymbol{\eta}', \omega'_d) \rangle, \quad (3.18)$$

where Π_s is the cross power spectrum density of the surface pressure fluctuations. With this substituted into (3.17), we can simplify the result to

$$\Pi(\mathbf{x}, \omega) = \frac{k_0^2 \hat{x}_i \hat{x}_j}{(4\pi R)^2 \Delta} \int_{s'} \int_{s'} n_i n'_j \Pi_s(\boldsymbol{\eta}, \boldsymbol{\eta}', \omega_d) e^{ik_0(\boldsymbol{\eta}' - \boldsymbol{\eta}) \cdot \hat{\mathbf{x}}} d^2 \boldsymbol{\eta} d^2 \boldsymbol{\eta}'. \quad (3.19)$$

The Doppler factor in this result comes from the ω' integration.

By the definition of mean square pressure fluctuations, we can now integrate the power spectrum density (3.19) within a particular frequency band to derive

$$\langle p^2 \rangle = \frac{1}{2\pi} \int_{\omega} \Pi(\mathbf{x}, \omega) d\omega, \quad (3.20)$$

where the mean squared pressure on the left hand side is to be understood as that for a particular frequency band and the integration with respect to ω on the right hand side is performed over that band. Thus, the result is a function of the center frequencies of the frequency bands. By substituting (3.19) into this, we find that

$$\langle p^2 \rangle = \frac{2\hat{x}_i \hat{x}_j}{(4\pi)^3 c_0^2 R^2 \Delta^4} \int_{s'} \int_{s'} n_i n'_j \int_{\omega_d} \omega_d^2 \Pi_s(\boldsymbol{\eta}, \boldsymbol{\eta}', \omega_d) e^{ik_0(\boldsymbol{\eta}' - \boldsymbol{\eta}) \cdot \hat{\mathbf{x}}} d\omega_d d^2 \boldsymbol{\eta} d^2 \boldsymbol{\eta}'. \quad (3.21)$$

Here, again, the integration with respect to ω_d on the right hand side is performed over a set of frequency bands so that the result is a function of the center frequencies of those bands. The 1/3 octave frequency bands can be a convenient choice. In cases where atmospheric absorption is to be included in the prediction, it is more suitable to choose narrow bands to define (3.21), because

of the significant variations of atmospheric absorption with frequency. This definition is followed here and the 1/3 octave band mean square pressure fluctuations will be computed by standard integration after the atmospheric absorption is applied to the narrow band results.

4. Scaling Laws

The analytical result (3.21) can be further reduced by dimensional analysis to derive scaling laws for the use of empirical prediction. To this end, we define a typical length scale ℓ_0 , time scale τ_0 and velocity scale u_0 , which are related to each other by

$$\ell_0 = u_0 \tau_0. \quad (4.1)$$

The velocity scale u_0 characterizes the unsteady motions of the flow and is usually different from the uniform velocity U of the moving landing gear. With these scaling parameters, we can define the Strouhal number by

$$St = f \ell_0 / U = \omega \ell_0 / (2\pi U), \quad (4.2)$$

where f denotes frequency and ω is the angular frequency defined in the previous section.

The cross spectrum density of the surface pressures is determined both by its amplitudes and by the coherence length of the cross spectrum. The former sets the scaling of the cross spectrum and the latter specifies the domain of significant contributions in the surface integrations in (3.21). Its amplitude can be scaled as

$$\Pi_s \sim (\rho_0 u_0^2)^2 \tau_0, \quad (4.3)$$

where ρ_0 is the constant mean density. Experimental studies in the past have shown that surface pressure fluctuations generated by unsteady flows are almost always orders of magnitudes smaller than the dynamic pressure of the mean flow ($\rho_0 U^2/2$). This means that the velocity scale u_0 defined here is much smaller than the mean flow velocity U .

Because the cross spectrum of the surface pressures is nonzero only within the coherent length, which is typically of the same order as ℓ_0 , the double surface integration in (3.21) is controlled by both the surface dimension and the coherence length scale. Thus, the double surface integration should be normalized by

$$d^2 \eta d^2 \eta' \sim \ell_0^2 S, \quad (4.4)$$

where S denotes the typical area of the body surface.

The terms in (3.21) that involve the scalar product of the far field location unit vector and the unit normal of the integration surface give the directivity of the generated noise. Thus, we can scale these terms as

$$\hat{x}_i \hat{x}_j n_i n'_j \sim D(\theta), \quad (4.5)$$

where D denotes the far field directivity, which is in general a function of the emission angle θ in the flyover plane and the azimuthal angle in the plane perpendicular to the flight path. The latter is not of interest to aircraft noise at landing conditions so that it is not considered here.

By normalizing the quantities in (3.21) with the scaling laws discussed above, we can rewrite the result as

$$\langle p^2 \rangle = (\rho_0 c_0^2)^2 M^6 D(\theta) \beta e^{-\alpha R} F(St) \frac{S}{R^2} \frac{1}{(1 - M \cos \theta)^4}. \quad (4.6)$$

where we have introduced new quantities α , β and F to denote respectively the attenuation due to atmospheric absorption, the radiation efficiency due to the production of unsteady flows by the steady motion of the landing gear and the normalized spectrum of the radiated noise. The first of these new quantities, α , is defined by decibels per length and is a function of frequency. It is introduced here because the results derived in the previous sections are for loss-less propagation. For practical applications where the propagation distance is usually many wavelengths, atmospheric absorption can significantly affect the amplitude of the noise received by the far field microphones so that it is included here. The second quantity, denoted by β , is essentially a radiation efficiency factor. It is defined by

$$\beta = u_0^3 / (4U^3). \quad (4.7)$$

This quantity measures the efficiency of energy conversion from the steady motion U of the body to the unsteady flows characterized by u_0 . The third quantity, the normalized spectrum F , is a function of the Strouhal number St defined by (4.2). Mathematically, this normalized spectrum is simply written for

$$F = \iint_{S' S} \frac{\hat{x}_i \hat{x}_j n_i n'_j}{D(\theta)} \int_{St_d} St_d^2 \frac{\Pi_s(St_d)}{(\rho_0 u_0^2) \tau_0} e^{ik_0(\eta' - \eta) \cdot \hat{x}} dSt_d \frac{d^2 \eta d^2 \eta'}{\ell_0^2 S}. \quad (4.8)$$

Since all quantities in this expression have been normalized with respective typical parameters, they should all have values of the order of unity. The normalized spectrum should thus also be of the order of unity. Clearly, the calculation of this spectrum requires detailed information on the surface pressure spectrum, which is usually not available in practical applications. For our empirical methods, this normalized spectrum will be modeled and calibrated by test data, which will be discussed in detail in the following sections.

The derivations that lead to the scaling law (4.6) show that it is a general result applicable to any individual parts in the landing gear assembly, from largest parts, the wheels, to the smallest dressings. The functional dependencies of the far field noise on the geometric and flow

parameters are summarized in Table 1. It is evident that some of the parametric dependencies are common to all parts. These include the dependence on ambient parameters, the sixth power law for Mach number, the spherical spreading of the noise, the convective amplification and the atmospheric absorption. The other functional dependencies in (4.6), such as the normalized spectrum, the radiation efficiency, the far field directivity and the surface of the integration, are component specific and may vary significantly. These component-specific quantities are also the ones that are difficult to define quantitatively, either by experimental studies or by analytical/numerical

Table 1 Functional dependencies of landing gear component noise.

Feature	Dependency
Ambient Medium	$(\rho_0 c_0^2)^2$
Mach Number	M^6
Spherical Spreading	R^{-2}
Convective Amplification	$(1 - M \cos \theta)^{-4}$
Atmospheric Absorption	$e^{-\alpha R}$
Directivity	$D(\theta)$
Radiation Efficiency	β
Component Size Effect	S
Spectrum	$F(St)$

calculations, essentially because of the variations in shapes, sizes and locations of the large number of parts in the gear assembly. These parametric dependencies can only be modeled empirically by correlating the scaling laws to experimental data.

Even in such an empirical approach, it is apparently very difficult to individually model every part that generates noise, which is a main reason why we follow the approach of cataloging the gear parts into three basic groups and decomposing the landing gear noise spectrum into three corresponding spectral components. The development of this model will be discussed in detail in the following sections. Clearly, it reduces the empirical modeling to three components, instead of all the individual parts in the gear assembly. The latter approach is in principle feasible, as followed in Ref 4, 5 and 8, where the total landing gear noise is predicted by building up the noise from the individual parts.

5. Empirical Prediction Schemes

Our empirical prediction schemes start with the hypothesis that landing gear noise can be decomposed into three spectral components respectively for the low, the mid and the high frequency domain, and the total noise is the incoherent energy summation of the three components. This enables us to express the total landing gear noise as

$$\langle p^2 \rangle = \langle p_L^2 \rangle + \langle p_M^2 \rangle + \langle p_H^2 \rangle \quad (5.1)$$

where the subscripts L , M and H respectively indicate the low, the mid and the high frequency component. This spectral decomposition has been discussed in detail before (Ref 6, 7 and 13). It results from a combination of data analyses of recent landing gear noise tests and source

mechanisms of the noise. Full configuration landing gear noise tests have shown that the far field noise has different spectral features and directivity characteristics in different frequency domains (also see Ref 15). This has been attributed to the noise generated by the three groups of landing gear parts, namely, the wheels, the main struts and the small details. The three groups have significantly different typical sizes, which makes their dominant noise well separated from each other in frequency. The spectral decomposition and the incoherent summation are the basis of the empirical methods reported in Ref 6 and 7, and are also the basic hypothesis of a statistical framework for landing gear noise prediction developed in Ref 13.

With the spectral decomposition (5.1), we can apply the result (4.6) to each of the three components. The normalized spectrum F is now defined as a function of the Strouhal number, based on the respective length scales in each spectral component. We choose the diameter of the wheels d , the average cross section dimension of the main struts a and the typical size of the small details ℓ as the length scales of respectively the low, the mid and the high frequency component. With this, the total landing gear noise can be written as

$$\langle p^2 \rangle = \frac{(\rho_0 c_0^2)^2 M^6 e^{-\alpha R} D_0(\theta)}{R^2 (1 - M \cos \theta)^4} \{P_L + P_M + P_H\}, \quad (5.2)$$

where features common to all components have been factored out and those that are component-specific are represented by the quantity P , with respective subscript for the three components. They are defined by

$$P = \beta S D(\theta) F(St). \quad (5.3)$$

Here the respective subscripts L , M and H should be used for all quantities to indicate the low, the mid and the high frequency component. The Strouhal number for each component is also defined by the corresponding characteristic length of each component. These results indicate that all three spectral components have their own individual directivity, but we have also included a directivity factor in (5.2), denoted by $D_0(\theta)$, to account for the installation effects. Thus, the directivity factors in (5.3) are for isolated landing gears and that in (5.2) accounts for the wing/fuselage reflection and other installation effects.

With the results (5.2) and (5.3), it only remains to empirically model the quantities on the right hand side of (5.2), respectively for the three frequency domains. This will be done by a combination of physical reasoning and calibration with test data. The flow energy conversion efficiency, denoted by β in (4.7), with respective subscripts for the three spectral components, can only be derived by matching predictions with test data. It basically describes how efficient the steady motion of the gear parts, at constant velocity U , generates unsteady flows characterized by the velocity scale u_0 , which in turn radiates noise. Thus, this quantity can also be regarded as a parameter to measure the noise radiation efficiency of the landing gear parts. By fitting the noise predictions to test data, we find a set of values for this parameter for the three

spectral components and these values are listed in Table 2. For empirical modeling, these values are basically empirical amplitudes of the component noise.

Table 2 Empirical amplitudes of the three landing gear noise components.

	Low	Mid	High
β	4.5×10^{-8}	1.5×10^{-8}	3.2×10^{-5}

The amplitude of each noise component is related to the aggregate surface area of the landing gear parts in each group, resulting from the surface pressure integration of the basic theory (3.21) and denoted by S with respective subscripts for the three spectral components. For the low frequency noise that is generated by the wheels, it is denoted by S_L and can be derived deterministically from the wheel dimensions. This leads to

$$S_L = \pi N_w w d, \quad (5.4)$$

where N_w is the number of wheels in the landing gear assembly, w is the wheel width and d is its diameter. It is clear that (5.4) does not account for the side surfaces of the wheels, because the normal of those surfaces is approximately perpendicular to the far field location vector in the flyover plane so that their noise contributions are negligible. The wheel diameter d is also used as the length scale for the low frequency noise, which defines the Strouhal number in the frequency domain according to

$$St_L = f d / U. \quad (5.5)$$

For the mid frequency component that is associated with the main struts in the landing gear, the aggregate effect of the surface pressure integration is denoted by S_M and can be computed as the summation of the surface areas of the main struts. The main struts are defined here as the elongated parts whose lengths are much larger than their cross section dimensions. They include the axels connecting the wheels, the shock struts connecting the wheel track to the aircraft, the side bars attached to the shock struts and the main hydraulic components. Under this definition, the surface of an individual part is the perimeter of the cross section multiplied by its length. For structural strength purpose, the main struts are usually designed with cross sections of either circular shape or rectangular shape. Though the struts of rectangular cross sections usually have cutouts so that they look more like I-beams or other cross sections, we will regard all non-circular struts as rectangular for simplicity, and account for the effects of cutouts and other irregularities in the high frequency components. Thus, we can define

$$S_M = \sum_{j=1}^{N_s} s_j L_j, \quad (5.6)$$

where s_j is the perimeter of the cross section of the j th strut, L_j is its length and N_s is the total number of main struts in the landing gear assembly. The perimeter of the cross section is defined by

$$s_j = \begin{cases} \pi d_j & \text{for circular cross section} \\ 2(a_j + b_j) & \text{for non - circular cross section} \end{cases} \quad (5.7)$$

where d_j is the diameter of the cross section if the j th strut is circular and a_j and b_j are its two linear dimensions if it is non-circular. The total length of the struts, denoted by L , is simply

$$L = \sum_{j=1}^{N_s} L_j. \quad (5.8)$$

The average dimension of the cross sections of the main struts is given by

$$a = S_M / (\pi L). \quad (5.9)$$

It can be seen that this is a weighted average, taking into account of the variations in the lengths of the struts. This is the quantity that is used as the length scale to define the mid frequency Strouhal number, namely,

$$St_M = f a / U. \quad (5.10)$$

It can be noted that the total number of main struts for the mid frequency noise component is not precisely defined, which for practical applications is not a significant uncertainty. The guideline is to include all large parts in the gear assembly, except the wheels, which are much larger in size than the small details. The latter is defined as those small parts such as brake braces, hydraulic hoses and wires, as well as small geometry irregularities such as cutouts and steps. As long as the large struts are included, the noise amplitude, proportional to the summation (5.6), will not be significantly affected by the addition of a few small parts.

For the high frequency component, the surface area calculation can in theory be carried out in a similar way to those used for the other two components, but this is clearly not practical, because of the large number of small parts and irregular geometric features in the gear assembly, which always have very different sizes, shapes and orientations. Thus, the aggregate effect of the surface integration for high frequency noise can only be modeled as a statistical quantity. The modeling of this quantity depends on the complexity of the small features in the landing gear, both the amount of small details and the relative locations of the small parts. To account for effects such as these, we model the aggregate surface integration effects in the high frequency domain as

$$S_H = \eta \ell^2, \quad (5.11)$$

where the length scale of the high frequency noise sources is denoted by ℓ and we have introduced a non-dimensional quantity, the complexity factor η , to account for the geometric

complexity of the large number of small parts in the landing gear. This latter quantity will be discussed and defined in detail in a later section.

The length scale of the high frequency noise source is used in (5.11) to reconcile the dimension of the surface quantity S_H . It is, however, an important parameter to define the Strouhal number in the high frequency domain,

$$St_H = f\ell/U. \quad (5.12)$$

For a given mean flow velocity, the length scale ℓ determines the frequency of the maximum high frequency noise, which in turn affects the levels of the total noise in the high frequency domain. This length scale can be taken as the typical size of the small geometric features in the landing gear, the average of the dimensions of the small features, for example. The small features include dressings attached to the main struts, standing-along parts such as brake braces, hydraulic hoses and wires, and small geometry irregularities such as cutouts and steps. Though a detailed survey is feasible to measure the sizes of the small features, it is by no means a trivial task, considering the large number of small details involved. It is then desirable to predefine a simpler way to obtain this length scale. In examining practical landing gears, we noticed that the sizes of the small details vary with the sizes of the large parts such as the main struts. Thus, we define the high frequency length scale simply by

$$\ell = 0.15a, \quad (5.13)$$

where a is the length scale for the mid frequency noise, defined by (5.9) as the length-weighted average dimension of the cross sections of the main struts. By using this definition, the task of measuring the large number of small details is avoided.

6. Normalized Spectra

The normalized spectra describe the frequency features of the landing gear noise in the three frequency domains. They are respectively determined by the three different noise generating groups of parts in the landing gear assembly, and each of them has its unique spectral characteristics. There are also general features that are common to all three components. They all achieve their maximum of unity at a value of the Strouhal number that characterizes the noise generation mechanisms, and they all fall off on both sides of the maximum at low and high Strouhal numbers. The falloffs have different rates for different spectral components. To accommodate features like these, a general form can be proposed for the normalized spectrum,

$$F(St) = A \frac{St^\sigma}{(B + St^\mu)^q}, \quad (6.1)$$

Where the indices σ , μ and q are empirical constants, which jointly define the spectral shape of the normalized spectrum, and A and B are parameters to ensure that F assumes its maximum of

unity at a value of the Strouhal number. We assume this general form for all three spectral components, but when applied to a particular component, a corresponding subscript should be used for the symbols.

Once the empirical constants σ , μ and q are given, by fitting with experimental data, for example, the parameters A and B can be determined analytically. By taking the derivative of the normalized spectrum F with respect to the Strouhal number St , it is straightforward to show that

$$\frac{dF}{dSt} = \frac{A St^{\sigma-1}}{(B + St^\mu)^{q+1}} \{ \sigma(B + St^\mu) - q\mu St^\mu \} \quad (6.2)$$

To require that the spectrum achieves maximum at the Strouhal number

$$St = St_0, \quad (6.3)$$

we can set the derivative (6.2) to zero at this Strouhal number, which in turn leads to the vanishing of the terms inside the brackets. This determines the value of B as

$$B = \{ (\mu q / \sigma) - 1 \} St_0^\mu. \quad (6.4)$$

The parameter A can now be determined by setting F to unity at the Strouhal number (6.3), which, after some straightforward algebra, leads to

$$A = (q\mu / \sigma)^q St_0^{q\mu-\sigma}. \quad (6.5)$$

The above discussions analytically determine the parameters A and B in terms of the indices μ and q and the value of St_0 which themselves need to be derived empirically. By analyzing trends in test data and curve-fitting the data, we find a set of values for these parameters, listed in Table 3 for all three noise components, together with those of A and B calculated by using (6.4) and (6.5). These values completely define the normalized spectra. For illustration, some examples of the three normalized spectra are plotted in Figure 2 as a function of frequency. In the examples, the flow Mach number is taken as 0.2 and the three length scales d , a and ℓ are respectively 40, 4 and 0.6 inches. The last, namely, the length scale for the high frequency noise, is calculated according to (5.13). The common features of the spectra are the unity maximum at the peak Strouhal number, and the falloff on

Table 3 Parameters to define the normalized spectra for the three landing gear noise components.

	Low	Mid	High
St_0	1.0	0.3	0.1
σ	4.0	3.0	2.0
μ	2.5	1.5	1.1
q	2.6	4.2	4.2
A	3.53	0.42	0.08
B	0.62	0.18	0.10

both sides of the maximum for both low and high values of Strouhal numbers. Since the three spectral components have different length scales, the spectral maximum are achieved at different frequencies. Also because of the three different length scales, the three spectra cover a wide range of frequencies.

The shapes and falloffs of the normalized spectra are controlled by the parameters, given in Table 3. From (6.1), it is clear that the low Strouhal number dependence of the spectrum is given by

$$F(St) \sim St^\sigma \quad \text{for } St \ll St_0, \quad (6.6)$$

and at large Strouhal numbers, the falloff follows

$$F(St) \sim St^{-(q\mu-\sigma)} \quad \text{for } St \gg St_0. \quad (6.7)$$

Since noise spectrum decreases at low and high frequencies away from the spectral maximum, the result (6.7) imposes a condition on the values of the indices, namely,

$$q\mu > \sigma. \quad (6.8)$$

Clearly, both are satisfied by the values given in Table 3.

The parameters μ and q also jointly define the width of the spectrum near the maximum frequency. It can be seen from Figure 2 that the low frequency component has the narrowest width and the high frequency component has the widest width with the mid frequency component in between the two. This means that the low frequency noise is narrow-banded and the noise becomes more broad-banded as frequency increases. This reflects the source physics of the three noise components and can be simply explained by the length scales of the three groups of landing gear parts that generate noise respectively in the three frequency domains. For the low frequency noise that is related to the wheels, there is only one size, namely, the wheel dimension, so that the noise spectrum is narrowly

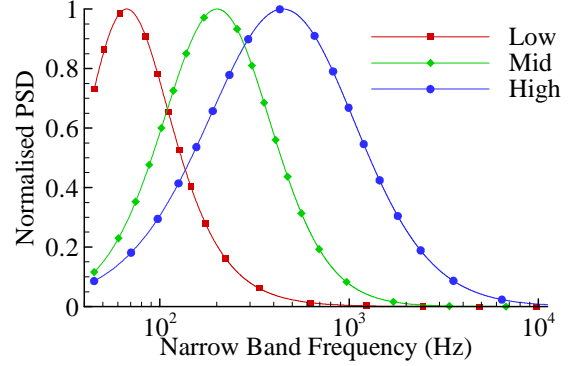


Figure 2 Illustration of the normalized power spectral density in the low, mid and high frequency domain.

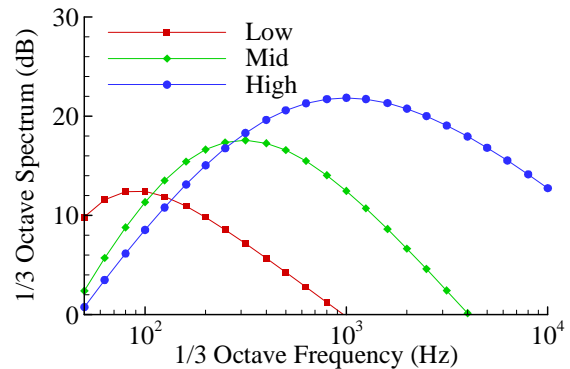


Figure 3 One third octave band levels of the three power spectral densities shown in Figure 2 respectively for the three frequency domains.

confined to frequencies near the vortex shedding frequency of the wheels. In the mid frequency domain, the parts that generate noise are the main struts which have a variety of sizes. Each of the struts may still radiate noise near its characteristic frequency, determined by the Strouhal number similarity rule, but the aggregate effects of the group of parts cover a range of frequencies, making the spectrum more broad-banded than a single part. The spectrum is even more broadened in the high frequency domain because the size distribution of the small parts in the landing gear covers an even wider range. All these are well illustrated in Figure 2. The normalized spectra defined by (6.1) lead to broadband 1/3 octave band sound pressure levels. This is demonstrated in Figure 3, where the 1/3 octave band results are simply integrated from the narrow band spectra plotted in Figure 2. The higher levels for the high frequency component result from the progressively wider 1/3 octave band width as frequency increases.

7. Directivity Factors

Test data have shown that noise from isolated landing gear in general follows a directivity pattern that peaks at the upstream and downstream direction and achieves minimum near the flyover location where the emission angle is approximately 90 degrees (*e.g.* Ref 7 and 15). This has also been observed in numerical simulations of landing gear noise using simple gear models (Ref 22 to 26). Detailed analyses of test data further reveal that the variations of far field noise with emission angle are also frequency-dependent. At low frequencies, the variations are very small and the radiation is almost omni-directional. As frequency increases, the radiation becomes more directional, showing variations of a few decibels in the mid and high frequency domain.

To account for this frequency dependent directivity, a general form is assumed for the directivity factor for the three spectral components,

$$D(\theta) = (1 + h \cos^2 \theta)^2, \quad (7.1)$$

where h is an empirical constant whose values are listed in Table 4 for the three landing gear noise components. When this general form is applied to a particular component, with corresponding values for the empirical constant, a subscript, L , M or H , should be used to identify the noise component, namely, the low, the mid or the high frequency component. The three directivity factors are plotted in Figure 4, as a function of the emission angle θ . The general features are that all three components have maximum in the upstream and downstream direction and minima at the flyover location at emission angle of 90 degrees. The differences between them are the amount of variations with emission angle. For the low frequency component, the variations are the smallest among the three, representing essentially omni directional radiation. The variations for the mid and high frequency component are more noticeable.

Table 4 Parameters defining the directivities of the three landing gear noise components.

Component	Low	Mid	High
h	0.2	0.6	1.0

These parametric trends are all empirically modeled and are all consistent with test data, including both isolated landing gears in wind tunnel tests and flight tests with full configuration aircraft. To demonstrate, the high frequency noise directivity is compared in Figure 5 with test data for the range of emission angle covered by the test data. The solid curve in this figure is the empirical model defined by (7.1) and the symbols are data, with the squares for the Boeing 737 two-wheel gear (Ref 7 and 16) and the circles for the Airbus 320 four-wheel gear (Ref 15). Both data sets are from wind tunnel tests and the details of the tests are described in the respective references. The Boeing 737 data are for the frequency domain from 1000 Hz to 13000 Hz, and the A320 data are for a range of Strouhal number from 4 to 12. In the latter case, the definition of the Strouhal number is given in Ref 15 and the range of 4 to 12 is described as the high frequency domain. Clearly, the comparison between the empirical model and the data shows good consistency.

The above discussions on the directivity variations of the three spectral components apply to isolated gears without the installation effects due to the reflection/diffraction from the aircraft wing and fuselage. The variations account for the directivities of individual sources, which are only one of the three elements that determine the overall far field noise directivity. The other two are the convective amplification, as already included in the model (5.2), and the installation effects. Thus, it only remains to model the installation effects to complete the modeling of far field directivity of the landing gear noise. There are only limited flight data available that can be used to extract the installation effects and there have been almost no studies on this by other approaches such as numerical simulations. Thus, once again, we will develop an empirical model from physical reasoning and calibration with available data. Intuitively, it is easy to see that the aircraft wing/fuselage reflection and diffraction will enhance the far field noise and this enhancement will be maximal at the overhead location and minimal in the flight direction. It is also clear that the maximum increase in far field noise due to the installation effects will be less than 3 dB, which would be achieved only from reflection of an infinite plate. To capture all these, we model the installation effects by

$$D_0(\theta) = 1.2 \times (1 - 0.9 \cos^2 \theta)^2. \quad (7.2)$$

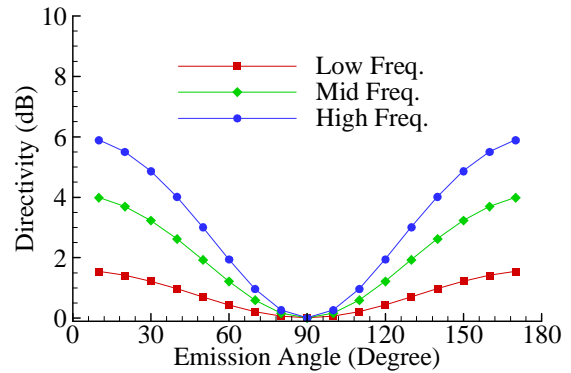


Figure 4 Models of the directivity factors for the three spectral components of landing gear noise.

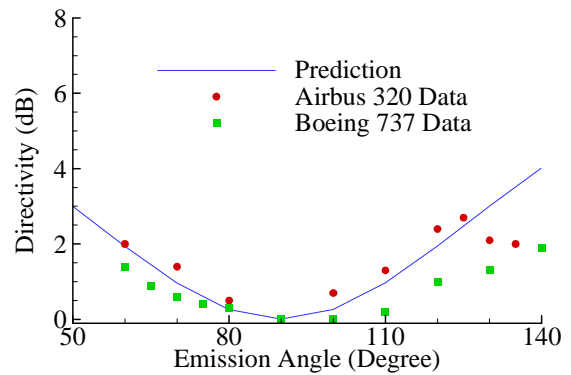


Figure 5 Comparison of empirical model with test data for the directivity of high frequency landing gear noise.

This gives about 0.8 dB of noise increase at the overhead location of 90 degrees of emission angle and the increase becomes negligible in the flow direction. The amount of noise increase at the overhead location in this model is entirely empirical, based only on the physical argument that the aircraft wing and fuselage provides some reflection and diffraction. We believe that this small amount of increase is reasonable for practical applications, though more detailed studies will be needed to define it more accurately.

Before detailed studies on the installation effects are available, the empirical model (7.2) can only be calibrated by test data. An example of such a calibration is shown in Figure 6, by using some flight test data of the Boeing 777 aircraft. As discussed before, the overall landing gear noise directivity contains three elements, the directivities of the individual sources, the convective amplification due to the motions of the sources and the installation effects. Since the Boeing 777 landing gear noise is dominated by the high frequency component, we plot the quantity

$$(1 - 0.9 \cos^2 \theta)^2 (1 + h_H \cos^2 \theta)^2, \quad (7.3)$$

as the overall directivity, with h_H given in Table 4. The flight test data are processed by extracting the convective amplification from the data and normalizing the results by the level at 90 degrees of emission angle. The empirical model seems to capture the trends of the far field noise pattern. The test data show significant scatter because the data was derived by subtracting the airframe noise, measured with landing gears retracted, from the total airframe noise, with both landing gears and other noise generating devices. This procedure usually works well in cases where the contributions from the two differ significantly, but involves uncertainties when the two are comparable. The latter is unfortunately the case.

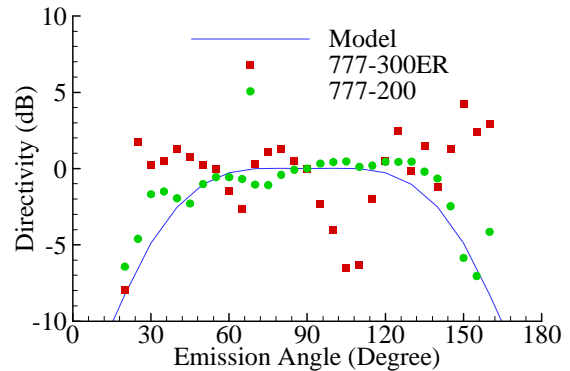


Figure 6 Overall far field directivity of the Boeing 777 landing gear noise.

8. Complexity Factor

To account for the large number of small features in the landing gear assembly, which is the source of high frequency noise, we have introduced a complexity factor in the empirical method, used in (5.11) to define the aggregate effects of surface integration over the surfaces of all the small parts. The qualitative description of this complexity factor is that it correlates the noise with the geometric complexity of the landing gear. The more complicated the landing gear assembly, the higher the noise levels. The geometric complexity of the landing gear is of course difficult to define quantitatively and uniquely. It can be related to aircraft operational parameters

such as the takeoff gross weight, or aerodynamic quantities such as the total drag of the landing gear, or the geometry of the gear such as its wheels and struts and their relative locations.

The aerodynamic parameters are attractive in relating the noise to its sources. The correlation of the complexity factor with the total drag of the landing gear is one way to define the complexity factor, because more complex landing gears correspondingly produce both more noise and more drag, because of the small, irregular geometric features. The drawback of this approach is that the total drag of a landing gear is not an easy quantity to obtain. In most cases, it has to be measured in wind tunnel tests. For this reason, we will not follow this approach, but will define the complexity factor from quantities that are easy to obtain from the landing gear geometry and the aircraft operation conditions.

It is easy to see that a significant source of geometric complexity, and hence, of landing gear high frequency noise, comes from the brake systems of the wheels, which are attached to the inner sides of the wheels with various parts of very irregular shapes and sizes. Since each wheel is equipped with such a system, the complexity factor for high frequency noise prediction can be assumed to increase with the number of wheels in the gear assembly. The more wheels the gear has, the more brake systems it needs, which in turn radiate more noise. The same reasoning applies to the main struts. There are hardly any clean struts in practical landing gears; most of them have cutouts and steps and they are almost always attached with braces, cables and wires. Thus, the more struts the gear assembly has, the more small details it has, and hence, the more noise it generates. The complexity factor for noise prediction can then be assumed to also increase with the total length of the main struts.

The complexity of the landing gear is not only related to the number of wheels and struts in the gear assembly, but also depends on the relative locations of the gear components. An example is the variations of landing gear noise with the alignment angle of the wheel track (see Figure 1 for the definition of wheel alignment angle) with respect to the flight direction. It has been observed that for the Boeing 777 aircraft, a noise reduction of 2 to 3 dB in a broad frequency range can be achieved by reducing the wheel track alignment angle from the conventional operational angle of 13 degrees to zero, making the wheel track align with the flow. This indicates the aerodynamic coupling of the noise generating components in the gear. This aerodynamic coupling of the landing gear sources is clearly difficult to study, but should be modeled in the empirical prediction.

There are of course geometric features that are not directly attached to the wheels and struts, hydraulic and cabling systems, for example. It is intuitive and logical to assume that larger aircraft requires more complex landing gears that have more complex geometric

Table 5 Examples of maximum gross takeoff weight for some aircraft types.

Aircraft	Max Takeoff Weight (lb)
717	110000
737	150000
747	840000
757	260000
767	420000
777	650000

features, which in turn generate more high frequency noise. Thus, it seems reasonable to correlate the complexity factor in noise prediction to the aircraft takeoff gross weight, which is an easily obtainable parameter in aircraft specifications. To illustrate, a list is given in Table 5 for some of the Boeing family airplanes. It should be pointed out that these are typical values for the aircraft types listed in this table. Within each aircraft type, there are usually various derivative airplanes with different maximum gross takeoff weight. The values listed here should only be used as a reference.

By considering all the discussions above, we define the complexity factor as an increasing function of the number of wheels in the gear, the total length of the main struts and the takeoff gross weight of the aircraft. It is also assumed to account for the effects of wheel track alignment. Thus, we define the complexity factor by the empirical model

$$\eta = \left\{ 1 + 0.028 \left(\frac{N_w}{N_{ref}} \frac{L}{L_{ref}} \frac{W}{W_{ref}} - 1 \right) \right\} \left\{ 1 + 2 \frac{N_w - 2}{N_w} \sin(2\gamma) \right\}, \quad (8.1)$$

where N_w and L have been previously defined respectively as the number of wheels and the total length of the main struts. We have used W to denote the maximum takeoff gross weight of the aircraft. The first bracket in (8.1) models the effects of geometric complexity of the landing gear and the second account for the effects of wheel track alignment, with γ denoting the alignment angle of the wheel track, equal to zero when the track is in the same direction as the flow. The subscript “*ref*” in (8.1) indicates reference quantities that are introduced to normalize the number of wheels, the total strut length and the maximum takeoff gross weight. The reference values are defined by

$$\begin{cases} N_{ref} = 2 \\ W_{ref} = 150000 \text{ lb} \\ L_{ref} = 300 \text{ in} \end{cases} \quad (8.2)$$

which are chosen such that the complexity factor η is approximately equal to unity for the Boeing 737 main landing gear. Since the reference values for the takeoff weight and the total strut length are given respectively in pounds and inches, the quantities W and L in (8.1) should also be specified in these two respective units.

From the empirical formula (8.1), the variations of the far field high frequency noise due to the complexity factor can be written in decibels by

$$\Delta SPL_\eta = 10 \log \left\{ 1 + 0.028 \left(\frac{N_w}{N_{ref}} \frac{L}{L_{ref}} \frac{W}{W_{ref}} - 1 \right) \right\} + 10 \log \left\{ 1 + 2 \frac{N_w - 2}{N_w} \sin(2\gamma) \right\}. \quad (8.3)$$

The first term on the right hand side is essentially the increment of high frequency landing gear noise due to geometric complexity of the gear and the second is that due to the wheel track alignment angle. The two are respectively plotted in Figure 8 and Figure 7. Both figures plot the increment in noise, with Figure 8 as a function of the combined effect of complexity features associated with the wheels, the struts and other, and Figure 7 as a function of the wheel track angle. The model for the geometric complexity groups together the brake systems, the attachments to the struts and other small features, respectively represented by the number of wheels, the total length of the struts and the gross takeoff weight. The model essentially assigns equal weighting to the three elements that affect the complexity factor. Though more elaborate models can be developed by correlating with test data from various landing gears, which are not currently available, we think the simple model given here should be sufficient for practical applications. This also holds for the empirical model for the wheel track angle effects; the model is basically calibrated by test data of the Boeing 777 main landing gear, which show a noise reduction of about 2 dB with the wheel track angle reduced from 13 degrees to zero.

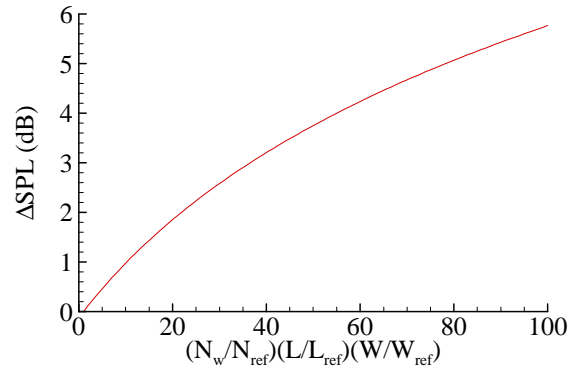


Figure 8 Increment of landing gear high frequency noise due to gear complexity.

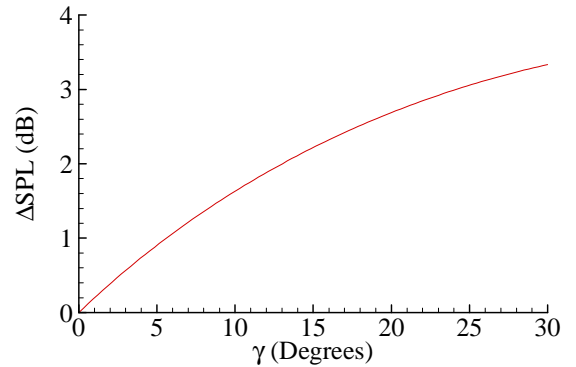


Figure 7 Increment of landing gear high frequency noise due to wheel track alignment angle.

9. Validation

In this section, we apply the empirical models developed in the previous sections to two cases to validate the models and to demonstrate their use in practical predictions. The first case is an isolated Boeing 737 main landing gear and the second is the total landing gear noise for the Boeing 777 aircraft. The latter includes contributions from both the main gears and the nose gear. For reference, the wheel dimensions for these two aircraft types are listed in Table 6. As in Table 5, the values are representative for the two respective aircraft types.

The test data for the isolated Boeing 737 main landing gear was obtained in the Boeing Low Speed Acoustic Facility (LSAF), where a

Table 6 Examples of wheel parameters.

Aircraft	Nose Gear		
	N_w	d (in)	w (in)
737	2	26	8
777	2	42	16
	Main Gear		
	N	d (in)	w (in)
737	2	42	16
777	6	50	20

Table 7 Typical dimensions of the main struts in the Boeing 737 main landing gear.

Component	Length (in)	Diameter/Width (in)	Thickness (in)
Shock Strut	76.0	8.5	-
Vertical Bar	27.0	5.5	1.0
Axel	18.0	7.0	-
Lower Side Bar	36.0	3.5	2.0
Upper Side Bar	30.0	3.5	2.0
Vertical Side Bar	13.0	2.0	1.6
Horizontal Side Bar	43.0	3.0	3.0
Upper Torque Bar	22.0	2.5	1.5
Lower Torque Bar	22.0	2.5	1.5
Junction Rod	13.0	1.5	-
Door Bar	10.0	2.0	1.5
Door Hydraulic Rod	7.0	1.5	-

full configuration gear was tested at various flow conditions. The test and the data analysis have been previously published (Ref 6, 7 and 16). The landing gear data was measured by an array of microphones along a straight line in the simulated fly-over plane at various emission angles. The distance between the center of the gear and the microphone at 90 degrees of emission angle is 10 feet. To apply the empirical models for the noise prediction, the dimensions of the main struts need to be supplied as input. For the Boeing 737 main landing gear, a typical list is given in Table 7, where the components

are circular in cross section if no numbers are listed in the last column. By using the definitions in section 4, the total length of the main struts is found to be 317 inches and the length scale for the mid frequency noise component is 4.65 inches. The latter also gives the length scale for the high frequency component as 0.7 inches, being 15 percent of the mid frequency length scale. Thus, we have

$$\begin{cases} L = 317 & \text{in} \\ a = 4.65 & \text{in} \\ \ell = 0.7 & \text{in} \end{cases} \quad (9.1)$$

for the main landing gear of the Boeing 737 aircraft.

By using the dimensions listed in Table 6 and Table 7, the predicted noise from an isolated Boeing 737 main landing gear is plotted in Figure 9, together with measured data. The plots are for the Sound Pressure Level (SPL) at three emission angles, as a function of frequency, for four flow Mach numbers. The distance from the gear center to the 90 degree microphone is 10 feet and that for the other two microphones is about 11.5 feet. The data shown in this figure are as measured and the predictions include the effects of atmospheric absorption, though those effects are small because of the small distances between the gear and the microphones. The test facility has a low frequency cutoff about 200 Hz so that no data below this frequency is shown in the figure. Since this is an isolated gear, the directivity factor $D_0(\theta)$ due to the installation effects is set to unity in the predictions. Also, because the data was from a wind tunnel test where the

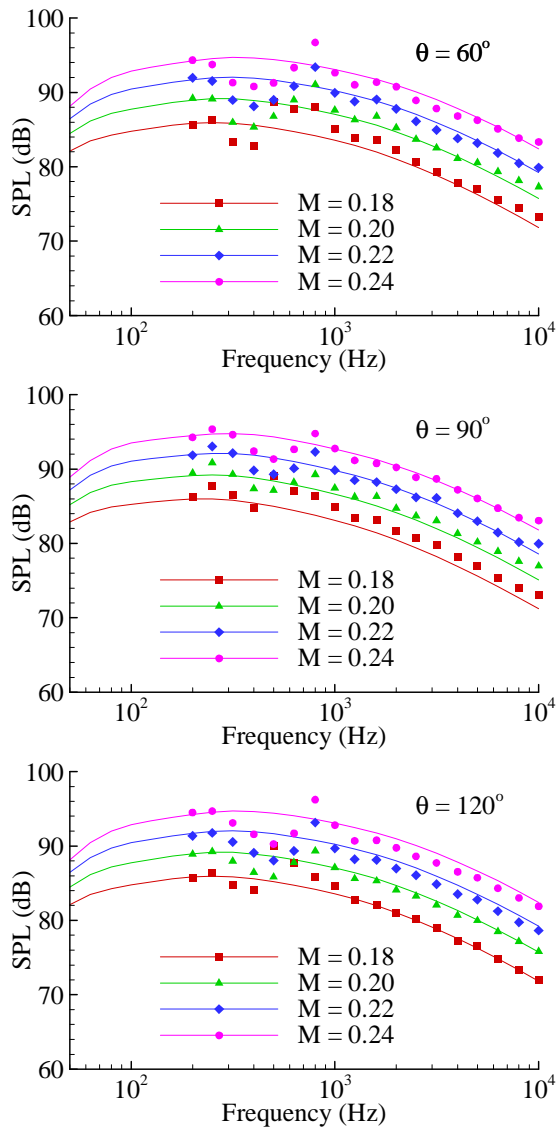


Figure 9 Comparison of SPL between predictions and test data for an isolated Boeing 737 main landing gear.

the comparison meaningful, the predicted OASPL is also computed for frequencies above 200 Hz. The overall agreements between predictions and data shown in Figure 9 and Figure 11 are satisfactory, but there are some discrepancies between the two, noticeably for the case of lowest Mach number of 0.18. This is due to the fact that the high frequency noise data scale on the seventh power in Mach number better than the sixth power. This is discussed in Ref 7 and is attributed to the significant contributions to the landing gear noise from the wake flow. This mechanism is not modeled here, as is clear in the development given in the previous sections, where the noise is scaled on the sixth power in Mach number. This approach is followed here because the difference is small enough to be acceptable for empirical predictions.

gear and the microphones are both fixed, there is no relative motion between the two and thus no effects due to convective amplification. For meaningful comparison, the predictions are done with the convective amplification removed. The comparisons between predictions and data show good agreement, which is expected since some of the empirical constants in the prediction models are calibrated by the data shown in this figure. It can be seen that there are consistent discrepancies of about a few dB between predictions and data in the frequency range of 800 to 1000 Hz. This is because the data are dominated by a tone caused by vortex shedding from a torque link, as analyzed in detail in Ref 7 and 16. This particular vortex tone is believed to be specific to this test and has not been observed in other measurements.

To illustrate the contributions from the three spectral components in the landing gear noise, Figure 10 plots the contributions from the three frequency domains, together with the total noise, for the Boeing 737 main gear at the overhead location with $M = 0.2$. In this case, the three components have comparable amplitudes, leading to a very broadband total noise spectrum. The overall noise levels are compared with data in Figure 11, for different flow Mach numbers, as a function of the emission angle. Again, the test data are for frequencies above 200 Hz because of the low frequency cutoff of the test facility. To make

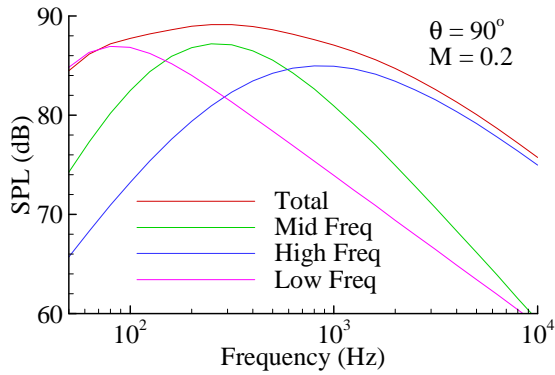


Figure 10 An example of spectral decomposition of total noise for the Boeing 737 main landing gear.

While the local flow velocity depends on the aircraft type and the location of the landing gear, we simply set it to 75 percent of the flight velocity here, due to the lack of detailed information on this parameter. Future work on this is clearly desirable and needed, since the noise is very sensitive to changes in the flow Mach number, scaling on the sixth power law. For the models used here, we define

$$M = 0.75M_0, \tag{9.2}$$

where M_0 denotes the flight Mach number and M is the local flow Mach number used in the prediction models developed in the previous sections.

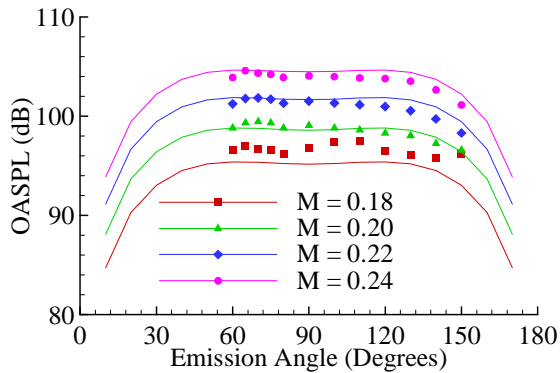


Figure 11 Comparison of OASPL between predictions and test data for an isolated Boeing 737 main landing gear.

For nose gear noise prediction, the complexity factor discussed in the previous sections also needs to be treated differently. The empirical models are developed based on main landing gears, which in general are more complicated and have more small details than nose gears. The gear complexity may not increase with parameters such as the maximum takeoff weight. Clearly, test data on nose gear noise are needed to develop a reliable model. This may turn out to be important because the flow velocity at the nose gear location is higher than that near the main gears, making significant contributions to the total noise. For the case considered here, we assume a

To apply the empirical models to the total aircraft landing gear noise, the contributions from the main gears and the nose gear need to be predicted independently and be added incoherently. Furthermore, the installation effects on the mean flow just ahead of the gear also need to be considered. This is because the local flow Mach number under the wing/fuselage can be different from the flight Mach number. From Ref 7 and 15, it is noted that for the main landing gear, the lifting effects of the wing typically reduce the local flow velocity to about 70 to 80 percent of the flight velocity.

This reduced local flow velocity may not apply to the nose gear that is under the fuselage. It is also possible that the local velocity may be even higher than the flight velocity because of the flow acceleration due to the nose geometry of the fuselage. This, however, needs to be confirmed. For the present application to the Boeing 777 aircraft as a demonstration, we assume the local flow velocity is the same as the flight velocity.

fixed value of 0.1 for the complexity factor. For reference, this is to be compared with the value of about unity for the Boeing 737 main landing gear. The small value assigned to the nose gear complexity factor reflects the fact that nose gears are much simpler than main gears and their complexity does not vary with aircraft type as much as main gears. This essentially suppresses the high frequency component and makes the low and mid frequency component dominant.

With these, we apply the empirical models to the Boeing 777 aircraft. The test data were obtained from flight tests at a flight Mach number of 0.258, with the data normalized to the aircraft noise certification condition, including the standard atmospheric absorption and the flight altitude of 394 feet. Again, the input for the predictions includes the wheel

parameters as well as the dimensions of the main struts, for both the main and the nose gear. These are listed in Table 8 and Table 9, respectively for the main and the nose gear. Apparently, the main gears are much more complex than the nose gear. This is especially true for the Boeing 777 aircraft because the main gears for this aircraft have six-wheel tracks. From these two tables, the total length of the struts and the length scales for the mid and high frequency component can be found from the definitions given in section 4, leading to

Table 8 Typical dimensions of the main struts in the Boeing 777 main landing gear.

Component	Length (in)	Diameter/Width (in)	Thickness (in)
Shock Strut	153.0	16.0	-
Upper Hydra. Rod	30.0	12.0	-
Lower Hydra. Rod	35.0	3.0	-
Axel	105.0	8.5	-
Axel Connection	120.0	13.0	-
Front Hydra. Rod	54.0	7.6	-
Low Front Side Bar	50.0	7.0	6.0
Lower Aft Side Bar	50.0	7.0	6.0
Up Front Side Bar	54.0	8.0	6.0
Upper Aft Side Bar	54.0	8.0	6.0
H. Front Side Bar	48.0	4.0	4.0
H. Aft Side Bar	43.0	4.0	4.0
Upper Torque Bar	58.0	5.0	3.0
Lower Torque Bar	64.0	5.0	3.0
Rear W. Steering	25.0	2.5	-
Rear W. Hydraulic	20.0	5.0	-

Table 9 Typical dimensions of main struts in the Boeing 777 nose gear assembly.

Component	Length (in)	Diameter/Width (in)	Thickness (in)
Shock Strut	75.0	9.0	-
Axel	20.0	6.0	-
Front Bar	42.0	4.0	4.0
Hydraulic Rod	9.0	3.5	-
Upper Torque Bar	58.0	5.0	3.0
Lower Torque Bar	64.0	5.0	3.0

$$\left\{ \begin{array}{l} L = 963 \text{ in} \\ a = 9.2 \text{ in} \\ \ell = 1.4 \text{ in} \end{array} \right. \text{ and } \left\{ \begin{array}{l} L = 268 \text{ in} \\ a = 6.2 \text{ in} \\ \ell = 0.9 \text{ in} \end{array} \right. \quad (9.3)$$

respectively for the Boeing 777 main and nose landing gear.

The prediction of the total landing gear noise for the Boeing 777 aircraft, including two six-wheel main gears and one two-wheel nose gear, is compared with test data in Figure 12, which plots the sound pressure levels at three emission angles as a function of frequency. The test data were obtained by taking the difference between two airframe noise measurements, one with and the other without the landing gears deployed. Because the landing gear noise for the Boeing 777 aircraft is comparable to other components of its airframe noise, the extracted landing gear noise data have uncertainties and this explains the significant scatter in the data, as evidently seen in Figure 12. Despite the scatter, the predictions seem to agree with the data well, both in the spectral shape and in the absolute noise levels. To illustrate the contributions respectively from the main and the nose gear, the case of 90 degrees emission angle is plotted in Figure 13, together with the individual contributions from the gears. The two main gears generate most of the total noise, with the nose gear contributing a small part in the low and mid frequency domain. This is expected because the main gears, with six wheels, for this aircraft type are much more complex than its nose gear. To further validate the empirical models, the overall sound pressure levels are predicted and compared with data in Figure 14, as a function of the emission angle. The overall trends of the test data are well captured by the predictions.

In the empirical models presented here, the landing gear noise prediction requires the dimensions of the main struts as input. These dimensions are not difficult to obtain. Since the predictions are not sensitive to small errors in the dimensions, an easy way to obtain them is to measure them on a production gear. The data

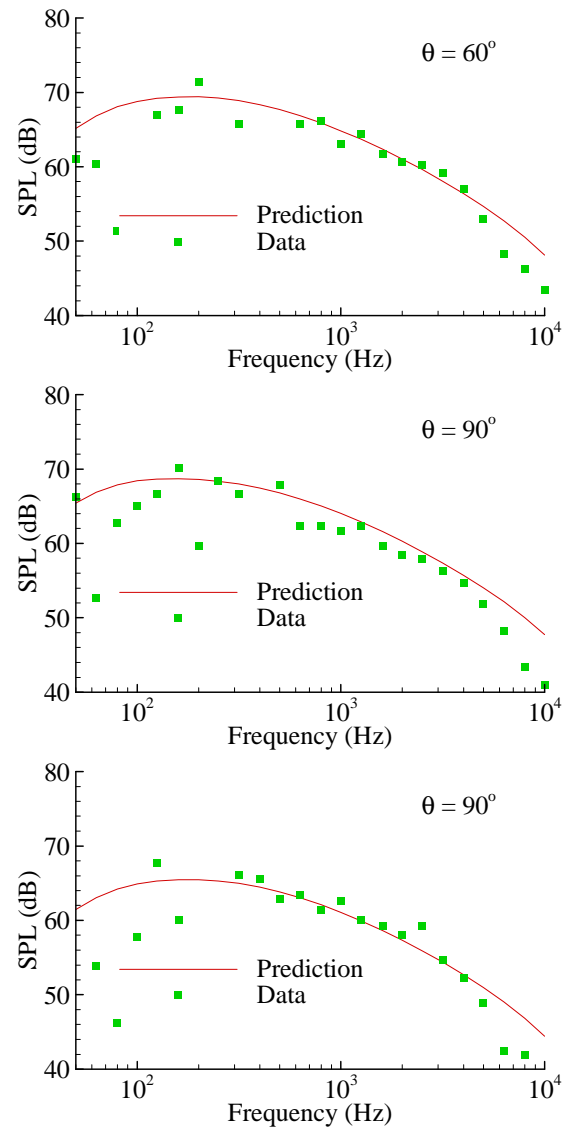


Figure 12 Comparison of landing gear noise SPL between predictions and test data for the Boeing 777 aircraft.

shown in this report are all obtained in this way. They contain some errors, compared with the values in the landing gear design charts, but these errors will only lead to insignificant differences in the prediction. There are practical cases where it may not be easy to obtain the dimensions of all the main struts, or where the noise prediction is performed only as an estimate without high accuracy requirement. In these cases, it is desirable if the predictions can be done by only specify one or two typical dimensions, instead of a whole list of the main struts. For this purpose, we recommend the use of the diameter of the shock strut, which is the component connecting the wheel track with the airframe and is usually the largest main strut in the gear assembly. With this diameter given, the total length of the main struts can be estimated by

$$L = 86d_s - 415, \quad (9.4)$$

where d_s denotes the diameter of the shock strut. This total length is needed for computing the mid frequency noise, as well as the complexity factor for the high frequency noise. Similarly, the length scale for the mid frequency noise component can be estimated by

$$a = 0.6d_s - 0.5. \quad (9.5)$$

For both quantities, the unit is inches. With this simplification, the quantity defined by (5.6) is replaced by

$$S_M = \pi a L, \quad (9.6)$$

which is needed in the calculation of the mid frequency noise. The two equations are derived from the data for the Boeing 777 and 737 aircraft main landing gear. They essentially assume that the size of the main struts scales on the size of the gear assembly. This is reasonable because the parts in the landing gear are designed to meet certain structural and operational requirements, which leads to large struts for large gears, and similarly, smaller struts for smaller gears. The equations can of course be improved by using more aircraft types, which, though not reported here, will be pursued in the near future.

10. Conclusions and Discussions

In this report, we have documented a semi-analytical and semi-empirical method for aircraft landing gear noise prediction. The method starts with the theory of aerodynamic sound

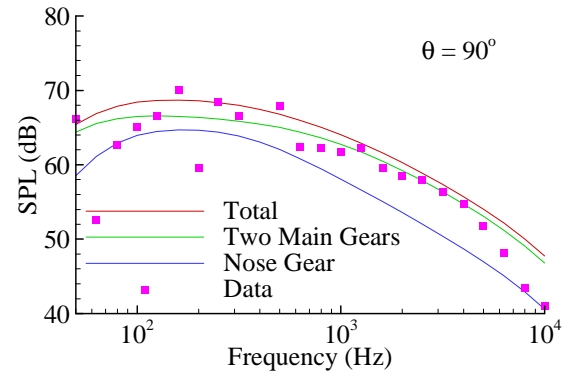


Figure 13 An example of the Boeing 777 aircraft landing gear noise and the contributions from its main and nose gear.

generation by moving bodies, which leads to scaling laws governing the functional dependencies of the far field noise from landing gears on aircraft operational parameters and landing gear geometric specifications. The total landing gear noise is decomposed into three spectral components, respectively for the low, the mid and the high frequency domain. The source mechanisms of these three components are respectively characterized by three groups of landing gear parts, namely, the wheels, the main struts and the small details of the gear assembly. Empirical modeling and correlation with test data are used to model the spectral properties and the far field noise directivity in the three frequency domains. The component modeling and prediction have been validated and calibrated by experimental data. The total landing gear noise predictions for the Boeing 737 and 777 aircraft have been compared with test data, showing good agreements both in parametric trends and in absolute noise levels.

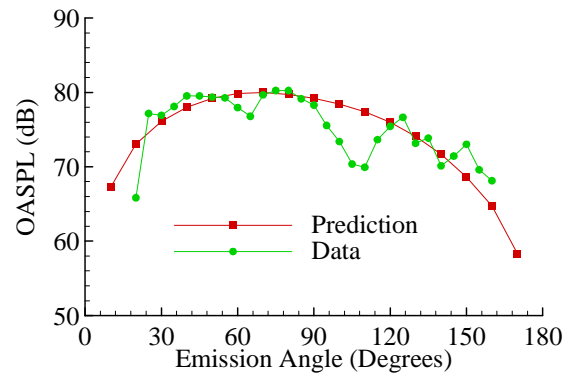


Figure 14 Comparison of OASPL between prediction and flight test data for the Boeing 777 landing gear noise.

11. Acknowledgments

The work reported here was conducted under NASA Contract NAS1-00086, under the Quiet Aircraft Technology (QAT) program. The author would like to thank the task monitor, Robert A. Golub of NASA LaRC, for his support and encouragement. The author would also like to thank Rob Stoker and Ronen Elkoby of the Boeing Company for their assistance in obtaining the test data and gear geometry, and for many helpful discussions on landing gear noise.

12. References

1. Fink M. R. "Airframe noise prediction method," *FAA-RD-77-29*, 1979.
2. Fink M. R. "Noise component method for airframe noise," *J. Aircraft* **16**(10), (1979) 659-665.
3. Crighton D. G. "Airframe Noise," *Aeroacoustics of flight Vehicles: Theory and Practice*. NASA RP-1258, **1** (1991) 391-447.
4. Smith M. G. and Chow L. C. "Prediction method fro aerodynamic noise from aircraft landing gear," *AIAA-98-2228*. June 1998.
5. Smith M. G. and Chow L. C. "Validation of a prediction model for aerodynamic noise from aircraft landing gear," *AIAA-2002-2581*. June 2002.
6. Sen R., Hardy B., Yamamoto K., Guo Y. P. & Miller G. "Airframe noise sub-component definition and model" NASA Informal Contract Report. NAS1-97040, 2000
7. Guo Y. P., Yamamoto K. J. and Stoker R. W. "An experimental study on aircraft landing gear noise" *J. Aircraft* (in press)

8. L. Lopes, K. Brentner, P. Morris, G. Lilley and D. Lockhard "Complex Landing Gear Noise Prediction Using a Simple Toolkit" AIAA-2005-1202 , Reno, Nevada, Jan. 2005
9. Ffowcs Williams J. E. & Hawkings D. L. "Sound generation by turbulence and surfaces in arbitrary motion" *Phil. Tran. Roy. Soc. Lond.* **A264**, 321, 1969.
10. Crighton D. G. "Basic principles of aerodynamic noise generation," *Progress in Aerospace Sciences* **16**(1) (1975) 31-96.
11. Lighthill M. J. "On sound generated aerodynamically I. General theory," *Proceedings of the Royal Society (London)*, **A 211** (1952) 564-587.
12. Crighton D. G., Dowling A. P., Ffowcs Williams J. E., Hekle M & Leppington F. G. *Modern Methods in Analytical Acoustics*. Springer-Verlag 1992.
13. Guo Y. P. "A statistical model for landing gear noise prediction," *J. Sound Vib.* (in press).
14. Heller H. and Dobrzynski W. "Sound radiation from aircraft wheel-well/landing-gear configuration," *J. Aircraft*, **14**(8), (1977) 768-774.
15. Dobrzynski W. and Buchholz H. "Full-scale noise testing on Airbus landing gears in the German Dutch Wind Tunnel," *AIAA- 97-1597*. May, 1997.
16. Stoker R. W. "*Landing Gear Noise Test Report*," NASA Contract NAS1-97040, 1997.
17. Michel U. and Qiao W. "Directivity of landing-gear noise based on flyover measurements" *AIAA-99-1956*, May 1999.
18. Dobrynski W., Chow L. C., Guion P. and Shiells D. "Research into landing gear airframe noise reduction," *AIAA-2002-2409*. June 2002.
19. Jaeger S. M., Burnside N. J., Soderman P. T., Horne W. C. and James K. D. "Microphone array assessment of an isolated 26%-scale high fidelity landing gear," *AIAA-2002-2410*. June 2002.
20. Horne W. C., James K. D. and Storms B. L. "Flow survey of the wake of a commercial transport main landing gear" *AIAA-2002-2407*, June 2002.
21. Chow L. C., Mau K. and Remy H. "Landing gear and high lift devices airframe noise research" *AIAA-2002-2408*, June 2002.
22. Hedges L. S., Travin A. and Spalart P. R. "Detached-Eddy Simulations over a simplified landing gear," *Journal of Fluids Engineering*, **124**(2), (2002) 413-423.
23. Li F., Khorrami M. R. and Malik M. R. "Unsteady simulation of a landing gear flow field," *AIAA-2002-2411*. June 2002.
24. Souliez F. J., Long L. N., Morris P. J. and Sharma A. "Landing gear aerodynamic noise prediction using unstructured grids," *AIAA-2002-0799*. June 2002.
25. D. Lockard and M. Khorrami "Aeroacoustic Analysis of a Simplified Landing Gear" AIAA-2003-3111, Hilton Head, South Carolina, May 2003
26. D. Lockard and M. Khorrami "High Resolution Calculation of a Simplified Landing Gear" AIAA-2004-2887, Manchester, United Kingdom, 2004

REPORT DOCUMENTATION PAGE

*Form Approved
OMB No. 0704-0188*

The public reporting burden for this collection of information is estimated to average 1 hour per response, including the time for reviewing instructions, searching existing data sources, gathering and maintaining the data needed, and completing and reviewing the collection of information. Send comments regarding this burden estimate or any other aspect of this collection of information, including suggestions for reducing this burden, to Department of Defense, Washington Headquarters Services, Directorate for Information Operations and Reports (0704-0188), 1215 Jefferson Davis Highway, Suite 1204, Arlington, VA 22202-4302. Respondents should be aware that notwithstanding any other provision of law, no person shall be subject to any penalty for failing to comply with a collection of information if it does not display a currently valid OMB control number.
PLEASE DO NOT RETURN YOUR FORM TO THE ABOVE ADDRESS.

1. REPORT DATE (DD-MM-YYYY) 01-07-2005		2. REPORT TYPE Contractor Report		3. DATES COVERED (From - To)	
4. TITLE AND SUBTITLE Empirical Prediction of Aircraft Landing Gear Noise				5a. CONTRACT NUMBER NAS1-00086	
				5b. GRANT NUMBER	
				5c. PROGRAM ELEMENT NUMBER	
6. AUTHOR(S) Guo, Yueping				5d. PROJECT NUMBER	
				5e. TASK NUMBER	
				5f. WORK UNIT NUMBER 23-781-20-12	
7. PERFORMING ORGANIZATION NAME(S) AND ADDRESS(ES) NASA Langley Research Center Boeing Phantom Works Hampton, VA 23681-2199 Long Beach, CA 90740				8. PERFORMING ORGANIZATION REPORT NUMBER	
9. SPONSORING/MONITORING AGENCY NAME(S) AND ADDRESS(ES) National Aeronautics and Space Administration Washington, DC 20546-0001				10. SPONSOR/MONITOR'S ACRONYM(S) NASA	
				11. SPONSOR/MONITOR'S REPORT NUMBER(S) NASA/CR-2005-213780	
12. DISTRIBUTION/AVAILABILITY STATEMENT Unclassified - Unlimited Subject Category 71 Availability: NASA CASI (301) 621-0390					
13. SUPPLEMENTARY NOTES Langley Technical Monitor: Robert A. Golub An electronic version can be found at http://ntrs.nasa.gov					
14. ABSTRACT <p>This report documents a semi-empirical/semi-analytical method for landing gear noise prediction. The method is based on scaling laws of the theory of aerodynamic noise generation and correlation of these scaling laws with current available test data. The former gives the method a sound theoretical foundation and the latter quantitatively determines the relations between the parameters of the landing gear assembly and the far field noise, enabling practical predictions of aircraft landing gear noise, both for parametric trends and for absolute noise levels. The prediction model is validated by wind tunnel test data for an isolated Boeing 737 landing gear and by flight data for the Boeing 777 airplane. In both cases, the predictions agree well with data, both in parametric trends and in absolute noise levels.</p>					
15. SUBJECT TERMS Acoustics; Aircraft noise; Gear Noise; Landing gear noise; Noise prediction; Airframe noise					
16. SECURITY CLASSIFICATION OF:			17. LIMITATION OF ABSTRACT	18. NUMBER OF PAGES	19a. NAME OF RESPONSIBLE PERSON
a. REPORT	b. ABSTRACT	c. THIS PAGE			STI Help Desk (email: help@sti.nasa.gov)
U	U	U	UU	38	19b. TELEPHONE NUMBER (Include area code) (301) 621-0390